ANNUAL REVIEWS

Annual Review of Nuclear and Particle Science

Ultra-High-Energy Gamma-Ray Astronomy

Zhen Cao,[1,2,3] Songzhan Chen,[1,2,3] Ruoyu Liu,[4,5] and Ruizhi Yang[6]

[1]Key Laboratory of Particle Astrophysics, Institute of High Energy Physics, Beijing, China; email: caozh@ihep.ac.cn

[2]Department of Physics, University of Chinese Academy of Sciences, Beijing, China

[3]Tianfu Cosmic Ray Research Center, Chengdu, China

[4]School of Astronomy and Space Science, Nanjing University, Nanjing, China

[5]Key Laboratory of Modern Astronomy and Astrophysics, Ministry of Education, Nanjing University, Nanjing, China

[6]Department of Astronomy, University of Science and Technology of China, Hefei, China

Annu. Rev. Nucl. Part. Sci. 2023. 73:341–63

First published as a Review in Advance on July 24, 2023

The *Annual Review of Nuclear and Particle Science* is online at nucl.annualreviews.org

https://doi.org/10.1146/annurev-nucl-112822-025357

Keywords

PeVatron, cosmic ray, gamma-ray, LHAASO, Crab Nebula, extensive air shower, muon content

Abstract

Ultra-high-energy (UHE, >0.1 PeV) γ-ray astronomy is rapidly evolving into an expanding branch of γ-ray astronomy with the surprising discovery of 12 PeVatrons and the detection of a handful of photons above 1 PeV. Nearly all known celestial object types that have emissions in the TeV band are found also to emit UHE photons. UHE γ-rays have a well-defined horizon inside our Galaxy due to the absorption of infrared and cosmic microwave backgrounds in the Universe. In the last 30 years, traditional cosmic ray (CR) measurement techniques have enabled the detection of UHE γ-rays and opened the last observation window. For leptonic sources, UHE radiation is in the deep Klein–Nishina regime, which is largely suppressed. Therefore, UHE γ-ray detection will be helpful in locating and identifying hadronic radiation sources, tracing the historic pursuit for the origin of CRs around the knee of the spectrum. The Crab Nebula is the focus of attention with measured photon emissions up to 1 PeV. In the absence of hadronic processes, these emissions may indicate the existence of an extreme accelerator of e^+e^-. Use of CR extensive air shower detection techniques broadens the field of view of the source

observations, enabling measurement of UHE radiation surrounding the sources. These observations can probe the particle propagation inside and outside the accelerators and the subsequent injection/escape into the interstellar medium.

Contents

1. INTRODUCTION

Very-high-energy (VHE) γ-ray astronomy has enabled enormous improvements in our understanding of the nonthermal Universe in the past three decades (1). From the detection of the first TeV photon from the Crab Nebula (2), there has been exponential growth not only in the number of observed sources that emit VHE γ-rays above 0.1 TeV but also in the types of astrophysical objects that can be considered possible sources of the VHE γ-ray emitters. New phenomena and radiation mechanisms constantly push the field forward to new territory with milestone discoveries (3). These discoveries make VHE γ-ray astronomy the most productive and successful subfield in the high-energy domain. This review focuses on photons with even higher energy, around 1 PeV; photons with energy above 0.1 PeV are called ultra-high-energy (UHE) photons. Historically,

many indications of photons above 1 PeV (4) drove a wave of development of γ-ray detection based on cosmic ray (CR) extensive air shower (EAS) measurement techniques. Detecting photons at 1 PeV provides the most direct evidence of the parent charged particles around 10 PeV in the sources. The acceleration mechanisms of these high-energy particles remain unclear after the discovery of CRs more than a century ago.

Following 30 years of development (5), techniques to detect UHE photons have matured with a sensitivity up to 10^{-14} TeV cm^{-2} s^{-1} at 0.1 PeV and effectively measure the emissions from many known VHE γ-ray sources, including the standard candle in the VHE domain, the Crab Nebula. Ushering in the era of UHE astronomy, the Large High Altitude Air Shower Observatory (LHAASO) (6), which is designed with a sensitivity of 12 milli-CU (Crab units, the flux from the Crab Nebula), rapidly discovered a dozen sources (7) with a stable flux of UHE photons brighter than 0.7 CU. Many of these sources have power-law-like spectral energy distributions (SEDs) without a clear cutoff feature. The upper limits of particle acceleration within Galactic sources were long assumed to be well below 1 PeV. These more recent discoveries have reset the upper limit to a much higher value, opening a broader territory of the nonthermal regime where there are many candidates for origins of CRs above 1 PeV (i.e., PeVatrons). New sources with unknown features, such as γ-ray morphological structures, have extended the field to explore new radiation mechanisms and particle acceleration procedures. The 12 UHE sources are conceivably associated with all types of known candidates, such as supernova remnants (SNRs), pulsar wind nebulae (PWNe), young massive-star clusters (YMCs), and microquasars. These sources currently are linked to VHE γ-ray emissions. More comprehensive surveys in the upcoming years will unveil new sources. In parallel, detailed investigations into known sources will continue.

This review is arranged as follows. Section 2 describes the domain of UHE γ-ray astronomy with a natural horizon due to absorption of the cosmic microwave background (CMB) and cosmic infrared background. Section 3 focuses on the development of the instruments and the critical technology, distinguishing between air showers induced by γ-rays and those induced by protons. Section 4 introduces the discovery of PeVatrons and possible candidate astrophysical object sources. Section 5 explains the deep investigation of the Crab Nebula, the best-studied object for its radiation and particle acceleration in the UHE domain, and focuses on the possible extreme acceleration of electrons and positrons. Section 6 discusses the most favorable candidates for CR factories, including the Cygnus region and SNR G106.3+2.7. Pulsar halos, a relatively new topic in spatially extended sources, are reviewed in Section 7, which considers both phenomenological and observational studies. Section 8 describes recent efforts to measure diffuse UHE γ-ray emissions from the Galactic Plane (GP) and their implications. Section 9 summarizes the review.

2. THE HIGHEST-ENERGY BAND OF ELECTROMAGNETIC OBSERVATION OF THE UNIVERSE

This section discusses the absorption of UHE photons through interactions with the low-energy background radiation fields that permeate the Universe, such as the CMB and the infrared background. We examine the sources of the UHE photons—notably, the PeVatrons and their definition, possible candidates, and distribution in the Universe. We also discuss PeVatrons as the origin of CRs and their relationship with the knee of the CR spectrum.

2.1. Absorption of Gamma-Rays in the Path to the Earth

High-energy γ-rays interact with the background photon fields inevitably via pair production ($\gamma\gamma \rightarrow e^+e^-$). In this process, γ-rays are attenuated. The CMB, the interstellar radiation field (ISRF) (8, 9) in our Galaxy, and the extragalactic background light (EBL) (10) contribute to the

background photon fields. The photon–photon pair production cross section averaged over directions of the background-radiation field depends on the product of energies of colliding photons. The energy dependence of the pair production cross section is given by Gould & Schréder (11). For a given energy of a γ-ray photon E_γ, it peaks at the wavelength of background photons $\lambda \sim 2.5(E_\gamma/1\ \mathrm{TeV})\ \mu\mathrm{m}$. The CMB is characterized as black-body radiation with a temperature of about 2.7 K, and its SED peaks at $\lambda \sim 1$ mm, while the EBL and ISRF are mainly contributed by the emissions from dust whose temperature is less than 100 K, and their SEDs peak at $\lambda \sim 100\ \mu\mathrm{m}$. In the local universe, the CMB starts to dominate the γ-ray opacity above 100 TeV, while the EBL dominates at lower energies. The opacity has been calculated by performing the line-of-sight integral of the product of the pair production cross section with the energy density of the radiation fields. The γ-ray opacity at 1 PeV is already larger than unity when the distance of the source is greater than 10 kpc, which means that we can hardly detect PeV photons of extragalactic origin. For 100-TeV photons, the mean-free path (at which distance the opacity is equal to 1) in typical EBL is estimated as 1.5 Mpc (9). Inside our Galaxy the ISRF also contributes significantly to the γ-ray opacity. Since the ISRF, unlike the EBL and CMB, is highly nonhomogeneously distributed in our Galaxy, the γ-ray opacity also depends strongly on the direction of sources. If the line of sight of a source passes through the Galactic Center (GC), the effect of the ISRF on 100-TeV γ-ray opacity approaches that of the EBL for the source at a distance of 1 Mpc, and the derived opacity is 0.7. In such a case, about half of the 100-TeV photons will be absorbed by the ISRF. We note that along this direction, a 100-TeV photon receives the largest possible attenuation in our Galaxy, and the opacity drops significantly as the latitude and longitude of the line of sight increase. At even lower energy, the opacity also drops sharply because the corresponding background photons below 100 TeV are dominated by the Wien side of the dust thermal emissions, whose number density drops significantly as the wavelength decreases (increasing background photon energy). At about 20 TeV, the ISRF is already transparent for γ-rays.

In conclusion, the CMB dominates the opacity for PeV photons and limits the horizon of PeV photons to our Galaxy. At 100 TeV, γ-ray sources are visible in the Local Group ($\sim$1 Mpc), and γ-rays from Galactic sources are only marginally attenuated if they locate toward the GC. Thus, the domain above 100 TeV is a suitable window for Galactic astronomy.

2.2. The Search Window for Galactic PeVatrons

The knee, a break in the energy spectrum of CRs measured at the Earth around 1 PeV (see, e.g., 12), is a significant feature. The current paradigm of CRs also postulates that at least to PeV-level energy, the CRs should have a Galactic origin (see, e.g., 13). Thus, one of the key issues in CR science is to identify the PeV particle accelerators, which are called PeVatrons, in our Galaxy.

CRs are charged particles and will be deflected by the Galactic magnetic field. As a rule-of-thumb estimation, the Larmor radius r_L can be estimated as follows:

$$r_\mathrm{L} \sim 10^{12}(E_p/1\ \mathrm{GeV})(B/3\ \mu\mathrm{G})^{-1}\ \mathrm{cm}, \qquad 1.$$

where E_p is the energy of the relativistic proton and B is the magnetic field. The magnetic field strength in our Galaxy lies in the range 1–10 μG, with an average value of 3 μG in the Galactic disk. Even for protons at energies as high as 1 PeV, R_L is only as small as approximately 1 pc assuming a magnetic field of 3 μG, which is much less than the distance to any possible CR source. As a result, the anisotropy in CR arrival direction measurements cannot provide decisive information on the CR sources. On the other hand, γ-rays, as the secondary production of CRs interacting with ambient gas, propagate rectilinearly and can be used to trace the CR acceleration sources. A γ-ray carries about one-tenth the energy of its parent CR (14); therefore, PeV CR protons are expected to produce γ-rays at energies of approximately 100 TeV, which is the UHE domain.

SNRs are regarded as the most promising CR accelerators in our Galaxy. GeV γ-ray observations have already identified the pion-decay feature of the γ-ray emission from middle-aged SNRs (15, 16), which is regarded as strong proof that these middle-aged SNRs do accelerate CR protons. However, every star like the Sun can generate particles up to energies above 10 GeV. The question of whether SNRs can account for the CRs up to PeV energies is still open. The middle-aged SNRs cannot be PeVatrons because the observed γ-ray spectrum reveals a cutoff at dozens of GeV, which corresponds to a cutoff in the parent proton spectrum around several hundred GeV. The younger SNRs are indeed TeV γ-ray emitters (17–20), but the production mechanism of these TeV γ-rays remains unclear. In this energy range, the γ-ray production mechanisms in the astrophysical process are inverse Compton (IC) scattering of relativistic electrons off low-energy background photon fields and neutral pion decay in the inelastic scattering of CR nuclei with ambient gas. When the energies of up-scattered photons exceed 100 TeV or so, the IC process enters the deep Klein–Nishina regime even if the target radiation field is the CMB. It therefore inevitably leads to a softening of the produced γ-ray spectrum at such high energies (21). Therefore, before LHAASO's operation, a hard spectrum above approximately 100 TeV without a significant softening could be formed only in a pion-decay process with a parent CR proton energy larger than several hundred TeV, which can be regarded as a strong hint of hadronic PeVatrons.

The above approach has been applied by the HESS Collaboration in the observation of HESS J1641-463 (21), in which a hard γ-ray spectrum with a spectral index of -2 extending to about 20 TeV is detected. Such a spectrum can be explained with an IC process only if the electron spectrum cutoff exceeds 700 TeV, which is extremely difficult in the corresponding SNR environment. On the other hand, the pion-decay process is a more natural explanation, and the observed γ-ray spectrum sets the 99% confidence level lower limit of the parent proton spectrum at 100 TeV. Clearly, high-precision γ-ray spectral measurements in an even higher UHE domain will reveal the origins of PeVatrons.

2.3. The Origin of Cosmic Rays Above the Knee

The origin of CRs above the knee (1 PeV or 10^{15} eV) is still unknown and is even more mysterious than that of CRs below the knee. For a CR around 10^{18} eV, the gyroradius (about 400 pc according to Equation 1) is comparable to the thickness of the Galactic disk. In this energy regime, two features have been identified in the CR spectrum: the second knee around $10^{17.5}$ eV, where the chemical composition changes significantly as measured by the HiRes detector (22), and the following dip (called the ankle) in the spectrum (23) around $10^{18.5}$ eV where the CR spectrum becomes flatter. The second knee is a significant break in the CR spectrum, at which the spectrum steepens from index -3.0 to approximately -3.3. It is widely accepted to be the upper limit of Galactic CR accelerators, such as SNRs, but it also could be consistent with the hypothesis that the CRs at higher energies escape more freely from the Galaxy (e.g., Reference 24). The hardening of the spectrum at the ankle is widely accepted to be an indication of the onset of the extragalactic component. What is the origin of CRs between the knee and ankle? Or, which portion of those CRs is accelerated by Galactic sources? What types of sources are responsible? All such questions are widely open, although the exact energy of the knee is still unclear because of the uncertainties of the chemical composition of CRs in this energy range. The UHE γ-ray observations, particularly the collections of photons above 1 PeV from different sources, seem quite promising in addressing these problems. First, the direct γ-ray observations can directly measure the maximum acceleration energies. Second, the diffuse γ-ray emissions from the GP and nearby giant molecular clouds provide independent measurements of CR spectra and chemical composition; since the γ-ray spectrum depends on kinetic energy per nucleon rather than on the total kinetic energy of the nucleus, different chemical compositions will produce different γ-ray spectra. In conclusion,

UHE γ-rays can provide unique and important information on the knee and on CR origins above the knee.

3. INSTRUMENTS OF ULTRA-HIGH-ENERGY GAMMA-RAY ASTRONOMY

In this section, we introduce existing instruments, ongoing projects, and impending detectors. Taking the historical point of view, we discuss the critical issue of CR background suppression techniques and how the EAS techniques developed into a successful γ-ray detection tool. Depending on the field of view of the instruments, they are used for two primary goals: surveying a large number of sources and making targeted observations for in-depth investigations regarding radiation mechanisms and particle accelerations in sources.

3.1. Historical and Technical Remarks About the Extensive Air Shower Technique in Gamma-Ray Astronomy

The technique of using a particle detector array to detect high-energy CR-particle-induced cascade processes has a long history of more than 70 years. Many particle detection techniques have been developed, such as the completely covered resistive plate chambers used in the ARGO-YBJ experiment (25); the water Cherenkov detectors in the Milagro (26), HAWC (27), and LHAASO-WCDA (28, 29) experiments; and the more widely used scintillator counters in the CASA-MIA (30), Tibet ASγ (31), and LHAASO-KM2A (28, 29) experiments. Photographs of the three current experiments at high altitude are shown in **Figure 1**. Timing the secondary particles that register each detector in the array at the surface with a precision of approximately 1 ns, one can reconstruct the EAS front and thus find the arrival direction of the primary particle. The angular

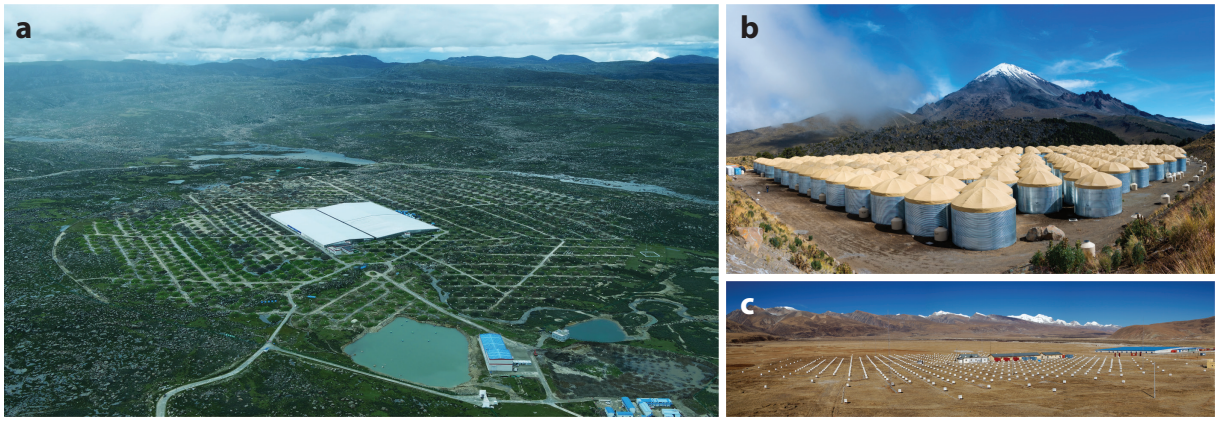

Figure 1

The three current experiments in ultra-high-energy γ-ray astronomy. Each experiment uses cosmic ray extensive air shower detection techniques. (*a*) Overview of the LHAASO detector array at Mt. Haizi (29°21′27.6″N, 100°08′19.6″E, 4,410 m above sea level) in China. The large structure in the middle of the array is the 78,000-m^2 WCDA. In the 1.3-km^2 circular area covered by the web of roads surrounding the WCDA, 5,216 scintillator counters and 1,188 muon detectors buried under soil humps form the KM2A. Panel reproduced with permission from the LHAASO Collaboration. (*b*) The HAWC array of 300 water tanks at Sierra Negra Volcano (18°59′41″N, 97°18′30″W, 4,100 m above sea level) in Mexico. The area of the array is approximately 20,000 m^2. Each tank has four photomultiplier tubes at 5 m beneath the water surface. Panel reproduced with permission from the HAWC Collaboration website (**https://www.hawc-observatory.org**). (*c*) The Tibet ASγ+MD array in Yangbajing (30°06′38″N, 90°31′50″E, 4,300 m above sea level). Panel reproduced with permission from the Tibet ASγ Collaboration. Abbreviations: KM2A, 1-km^2 array; WCDA, water Cherenkov detector array.

resolution strongly depends on how many detectors are registered in an EAS event. The number of particles recorded in the detectors allows one to determine the energy of the primary particle being reconstructed. The fill factor of the active detector area to the total area covered by the array plays an important role in maintaining a high resolution. However, the ultimate limit to the angular resolution is set by the intrinsic fluctuations of the arrival time of particles in the shower front. The altitude at which the EAS array is situated is found to be crucial as well. At more than 4,300 m above sea level, the detector arrays are close enough to the shower maximum that the shower fluctuations around 1 PeV are minimized. The shower detection threshold is lowered at higher sites as well. However, if this technique is used for γ-ray detection, the very high level of diffuse CR background is still a major difficulty. Even for the brightest point-like sources, such as the Crab Nebula, the photon signal flux is lower than the CR background in the point spread function (PSF) by orders of magnitude. Up to the second decade of the 2000s, this essentially set the limit of sensitivities of the detectors to worse than about 1 CU (see **Figure 2*b***) in γ-ray detection, even for a mega-scale array like CASA-MIA with a size of 1/4 km^2 (not shown in **Figure 2**).

3.2. Cosmic Ray Background Suppression Techniques and Capabilities

In principle, the μ content of a shower is a clear veto to suppress the CR background. In showers induced by CRs, the multiparticle production generates a large number of muons. In contrast, because of the very small photoproduction cross section in pure electromagnetic cascade induced by a primary photon, only small μ content is expected. In practice, to realize effective vetoing by measuring such small μ content, a quite significant fill factor of muon detectors is required, and therefore it is very difficult. For instance, the ∼1% fill factor of active muon detectors in the CASA-MIA experiment was found not to be sufficient. An economically affordable solution of μ content measurement was needed and developed in the past two decades. In the second generation of EAS detector arrays, the Tibet ASγ+MD (32) experiment as well as the HAWC experiment combined the two key features of the EAS detection—namely, the high altitude (>4,000 m above sea level) and the effective μ content measurement with a fill factor of 5%—and thereby successfully boosted the sensitivity of γ-ray detection by a factor of 10. Almost at the same time, the LHAASO design was approved in 2015 with a combination of a 78,000-m^2 water Cherenkov detector array (WCDA), which has a typical CR background rejection power of 10^{-3}, and a 1-km^2 scintillator counter array (KM2A), in which 1,188 muon detectors with a total active area of 40,000 m^2 are uniformly distributed. The CR background rejection power reaches 10^{-4} at 100 TeV and 10^{-5} above 500 TeV (see **Figure 2*a***). The 15-m spacing between counters in KM2A and the 5 × 5 m^2 cells in WCDA provide an angular resolution of 0.2° at 10 TeV for WCDA and above 400 TeV for KM2A. Each detector in the array is equipped with the White Rabbit protocol–based clock distribution system by which the clocks in the detectors are synchronized with an accuracy of 0.2 ns. The state-of-the-art sensitivity of γ-ray source detection by LHAASO reaches a level of 0.012 CU, as shown in **Figure 2*b***. With an-order-of-magnitude improvement in sensitivity above 50 TeV compared with that of the previous-generation experiments, LHAASO (29) has become the leading instrument in UHE γ-ray astronomy.

3.3. Survey for Sources and Targeted Observation for Deep Investigations

The field of view of an EAS array typically covers one-sixth of the sky at any moment. The operation duty cycle is typically greater than 95%. Thus, EAS arrays are ideal for sky surveys for γ-ray sources and particularly for the extended sources. The HAWC Collaboration has published a catalog of VHE sources in the GP (42). LHAASO, which operates in a higher-energy range, will release its catalog soon. Using half of the observatory's designed capacity, the LHAASO

Collaboration found 12 Galactic UHE γ-ray sources in 11 months of data taking (7). Most of the observed sources were extended, so multiple individual objects could be potentially associated with each of the UHE γ-ray sources. A better angular resolution than that of the EAS array is needed for further investigation of the origin of the UHE photons. The r_{68} of the PSF, which is defined as the radius inside which 68% of the photons from the point source are contained, is about 0.2° for HAWC above 10 TeV and for LHAASO-KM2A above 100 TeV (43). The r_{68} of imaging air Cherenkov telescope arrays (IACTs) is typically 2 arcminutes, which is five times better than that of EAS arrays. Thus, IACTs are ideal instruments to complement the EAS arrays for targeted

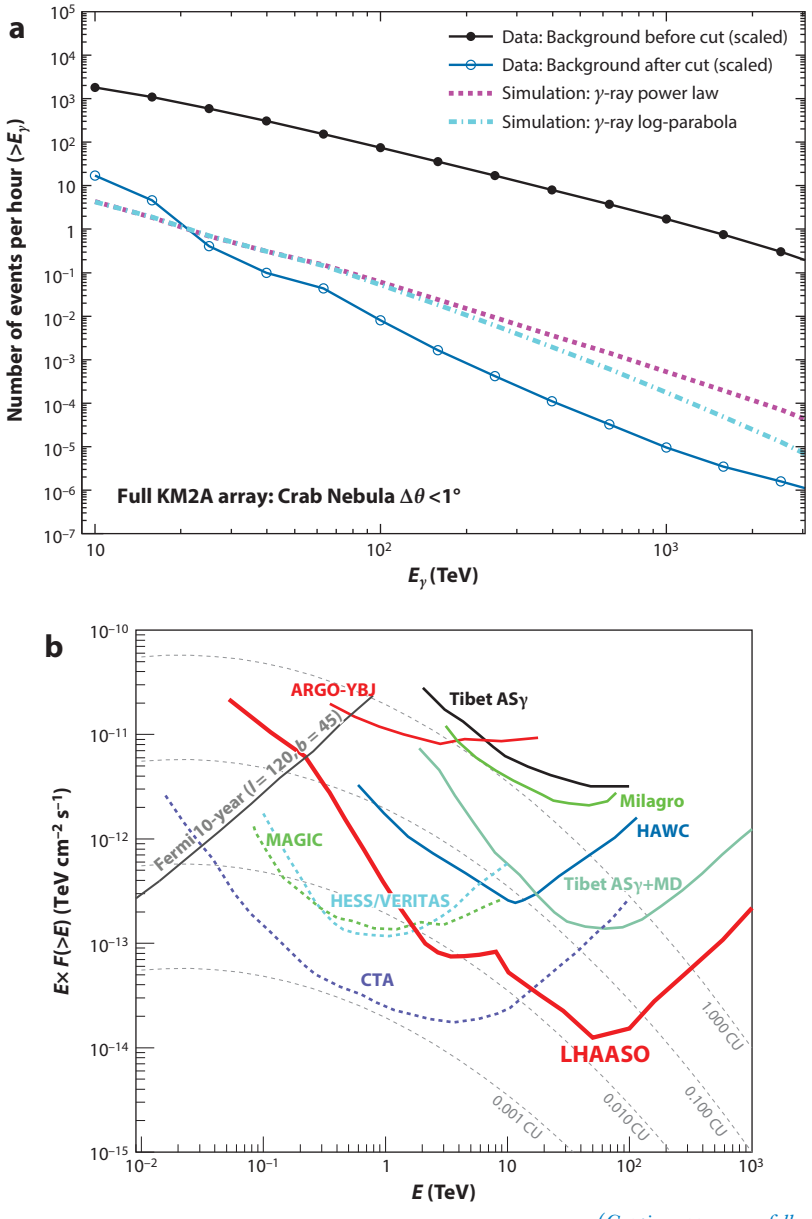

(*Caption appears on following page*)

Figure 2 (*Figure appears on preceding page*)

(*a*) The rates of detection of γ-rays from the Crab Nebula and the CR background events above the shower energy E_γ by the LHAASO-KM2A array in a cone of 1° centered on the Crab Nebula. The cyan dashed–dotted and pink dashed lines represent the integrated rates of detected γ-rays from the Crab Nebula based on log-parabola and power-law models fitted to the measured fluxes, respectively. Black filled circles show the integrated rate of CR events before applying a muon-less cut. Blue open circles represent the integrated rate of remaining CR events after applying the muon-less-cut filter. Panel adapted with permission from Reference 33. (*b*) Sensitivities of very-high-energy and ultra-high-energy γ-ray astronomical instruments as functions of γ-ray energy, *E*. The Crab Nebula spectral energy distribution in log-parabola functional form (*gray short dashed lines*) is a global fitting of all the measurements presented in figure 3 of Reference 33. The ground-based EAS array experiments Tibet ASγ and Tibet ASγ+MD (34), ARGO-YBJ (35), Milagro and HAWC (36), and LHAASO (37) are represented by colored solid lines. The IACT experiments CTA (38), VERITAS and HESS (39), and MAGIC (40) are represented by colored dotted lines. The 10-year sensitivity of Fermi-LAT (41) is represented by the gray solid line. Abbreviations: CR, cosmic ray; EAS, extensive air shower; IACT, imaging air Cherenkov telescope array; KM2A, 1-km^2 array.

observations. However, because of the small effective acceptance of the existing IACTs, no source to date has been firmly detected by IACTs in UHE domain. Next-generation IACT experiments, such as CTA and particularly the newly proposed ASTRI (44) and LACT, will be equipped with more telescopes to enhance the collection area up to approximately 10^6 m^2 and to have good synergy with current EAS arrays, and will perform targeted observations in depth toward the UHE sources. The other aspect of the UHE γ-ray astronomical observation is that only the Northern Sky is covered by the surveying instruments. The newly proposed Southern Wide-field Gamma-ray Observatory (SWGO) (45) is an EAS detection instrument located at a high-altitude site in the Southern Hemisphere with similar or even better sensitivity than that of LHAASO. Many UHE sources are expected to be discovered in the inner part of our Galaxy including the GC.

4. DISCOVERY OF PEVATRONS

One of the most important topics in γ-ray astronomy is the search for PeVatrons. Progress has been made in recent years. The first hint was provided by the HESS experiment, which measured a hard SED up to 20 TeV (46). Subsequently, more direct clues came from the Tibet ASγ and HAWC experiments with small numbers of UHE γ-rays collected (47, 48) and a photon at approximately 0.4 PeV recorded by the former (47). By 2021, concrete evidence regarding PeVatrons had been found by LHAASO (7), which detected 534 UHE γ-ray photons up to energies of 1.4 PeV. Both the maximum energy and the number of UHE photons will have increased by the time this review is published. In this section, we review the search for PeVatrons and discuss various types of possible astrophysical candidates. Three specific promising PeVatron candidates will be further discussed in Sections 5 and 6.

4.1. The First Hint from the Galactic Center

As mentioned in Section 2.2, the method used before the LHAASO era to hunt PeVatrons was to search for the hard γ-ray spectrum above approximately 100 TeV without significant softening. Before 2021, the strongest hint came from the HESS observations on the GC region (46, 49). The VHE emissions in the GC can be decomposed into three components: one bright central point source, the point source associated with SNR G0.9+0.1, and the diffuse emissions associated with the gas distributions (50). The spectrum of the central point source has a significant cutoff at several TeV. However, the diffuse emissions have a hard spectrum (index of about 2.3) and show no hint of cutoff up to more than 20 TeV (46, 49). The diffuse γ-ray spectrum indicates that the 90% lower limit of the cutoff in parent CR protons is 0.6 PeV. Furthermore, the HESS Collaboration

also derived the CR radial distribution with respect to GC by using the γ-ray flux measurement and the gas distribution based on molecular line emissions. The derived CR spatial distribution is consistent with a $1/r$ profile, which is expected assuming that the CRs are injected continuously from the central region with a size of tens of parsecs at the center of our Galaxy. The possible accelerator may be the supermassive black hole Sagittarius A* itself (46) or the YMCs, such as Arches, Nuclear cluster, and Quintuplet, which are all located in the central region.

Although the HESS results found strong hints of possible PeVatrons in the GC region, we note that the 90% lower limit of the cutoff in parent CR protons is 0.6 PeV, while the 95% lower limit is only 0.4 PeV. Indeed, the cutoff energy E_c in the γ-ray spectrum reflects the cutoff in the parent proton spectrum of about 10–20 E_c (14). And the observation by the MAGIC Collaboration (51) in the same regions found hints of a spectral cutoff, which is in contradiction to the measurements of the HESS and VERITAS experiments. More solid identification of PeVatrons requires accurate spectral measurement above 100 TeV—that is, the UHE domain in which IACTs do not have sufficient sensitivity.

4.2. Discovery of the First Group of PeVatrons with the Flux ∼1 Crab Unit

Before 2021, several Galactic sources were observed with γ-ray energies slightly higher than 0.1 PeV by the Tibet ASγ (47), HAWC (48), and MAGIC (52) experiments. These observations provide more direct hints of the existence of Galactic PeVatrons. However, unbiased identification and in-depth investigation of PeVatrons require detection of steady γ-ray fluxes with energies well above 0.1 PeV for hadron PeVatrons. Alternatively, a stable γ-ray flux above 0.4 PeV must be detected for a lepton PeVatron, if it exists, where the IC scattering of a parent electron generates approximately $0.4(E_e/\mathrm{PeV})^{1.3}$ PeV photons with an energy of E_e.

In 2021, the LHAASO Collaboration reported the detection of more than 500 photons at energies above 100 TeV that form 12 clear clusters in the sky with statistical significance $>7\sigma$ for each one, thus revealing UHE γ-ray sources (7). This marked the discovery of the first group of PeVatrons. The most energetic γ-ray was found at 1.4 PeV from the Cygnus region. As shown in the significance map in **Figure 3**, the 12 sources line up with good coincidence with the GP. Most of those UHE γ-ray sources are associated with known VHE sources. This suggests that the Milky Way is likely full of PeVatrons.

Among the 12 UHE sources, 8 were found to emit γ-rays more energetic than 0.4 PeV. Several potential counterparts are found in their proximity, including PWNe, SNRs, and star-forming regions; however, except for the Crab Nebula, the production sites have not yet been confirmed (7). Further in-depth investigations, particularly multiwavelength analyses, will help identify the relevant candidates accounting for the PeVatrons.

LHAASO also measured the SEDs of the three most luminous sources: LHAASO J1825-1326, LHAASO J1908+0621, and LHAASO J2226+6057. Despite the steep spectra of these sources, no clear cutoff features have been found below 500 TeV. For all sources, the absorption due to the ISRF and CMB is found to be small, even for the photons at the highest energies. The SEDs of γ-rays almost directly represent the parent particle energy distributions in the PeVatrons, and therefore they are crucial for revealing the corresponding particle acceleration mechanism. Further phenomenological studies have been conducted to localize and identify the PeVatrons, as briefly summarized in the subsections below.

4.3. Possible Astrophysical Counterparts of PeVatrons

UHE γ-ray observations indicate that astrophysical objects associated with PeVatron candidates seem related to violent explosions or energetic outflows. Here, we briefly introduce the main astrophysical candidates for Galactic PeVatrons.

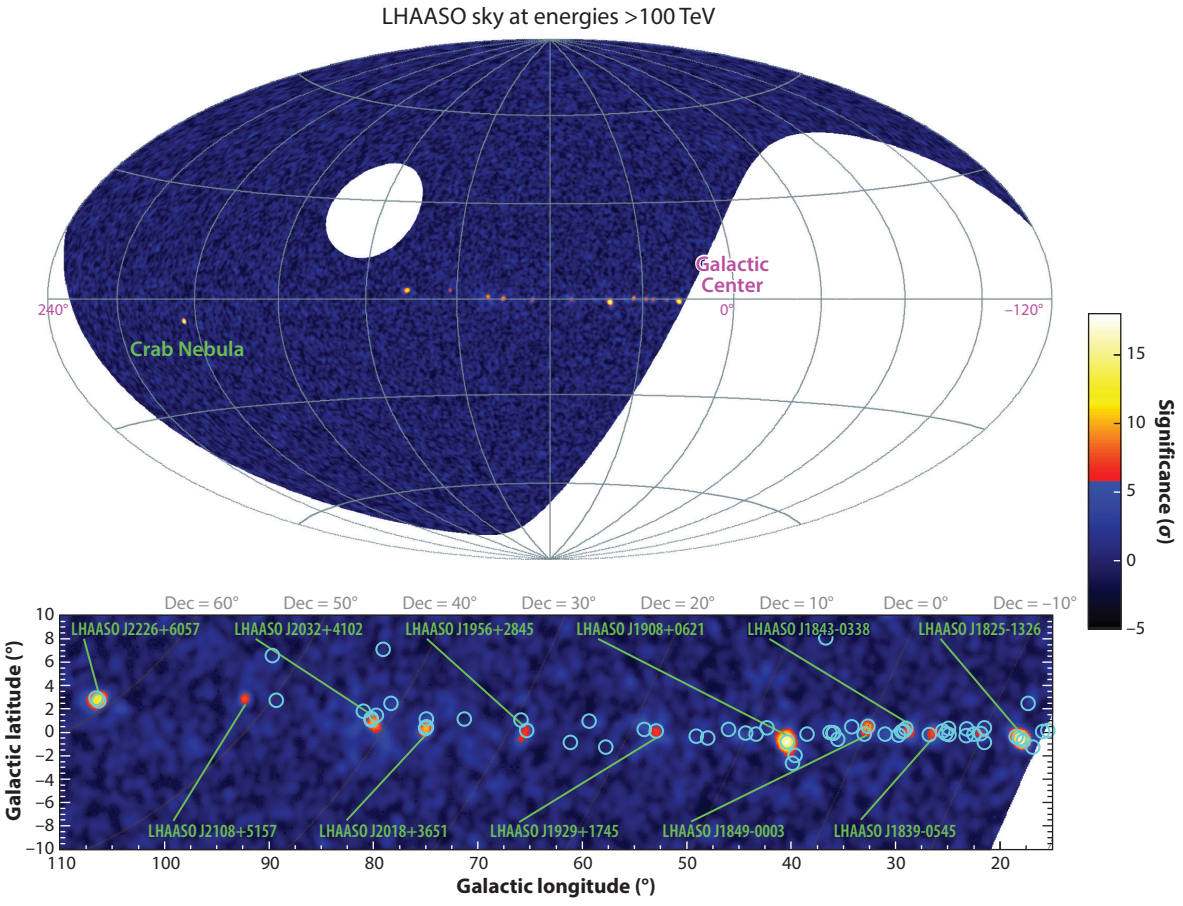

Figure 3

LHAASO sky map at energies above 100 TeV. The blue open circles in the lower subpanel indicate the positions of known very-high-energy γ-ray sources. Figure adapted with permission from Reference 7.

4.3.1. Pulsar wind nebulae. PWNe are powered by energetic pulsars, which are composed of electrons and positrons driven from the magnetosphere. These particles form a cold ultrarelativistic wind and are further accelerated at the termination shock generated when the pulsar wind encounters the ambient medium (53). PWNe have been recognized as one of the most efficient types of electron factories in the Galaxy. PWNe account for a large fraction of identified Galactic VHE sources. It is widely believed that the high-energy γ-ray emission of PWNe mainly comes from IC scattering of the high-energy electrons and positrons on ambient low-energy photons, such as the infrared ISRF and the CMB. However, hadronic processes are also suggested as possibly responsible for the γ-ray emissions, particularly at the high-energy ends of SEDs (see detailed discussion in Section 5.2).

Among the 12 UHE sources detected by LHAASO, the only firmly identified one is the Crab Nebula, which is widely known as a PWN.[1] In a deep investigation, the LHAASO Collaboration

[1]The Crab Nebula (as well as some other PWNe) is sometimes also called an SNR because it forms after a supernova explosion. We refer to it here as a PWN based on the physical origin of its radiation, which is produced by electrons and positrons blown from the pulsar.

reported the SED of the Crab Nebula extending to 1.1 PeV following a simple log-parabola functional form with an index of -3.12 ± 0.03 around 1 PeV (33). A detailed discussion of the Crab Nebula can be found in Section 5.

In the vicinity of every single LHAASO-detected UHE source except for LHAASO J2108+5157, there is at least one energetic pulsar with spin-down power above 10^{35} erg s^{-1} (more detailed discussion can be found in Reference 54, according to which the maximum attainable electron energy in each PWN can account for LHAASO's observation, except for the one in the Cygnus region—i.e., LHAASO J2032+4102). Such a strong correlation indicates that PWNe are very likely UHE sources, and thus there might be potential candidates for PeV accelerators among them.

Recent observations of the HAWC J1826-128 (55) (spatially coincident with LHAASO J1825-1326) and MGRO J1908+06 (56) (coincident with LHAASO J1908+0621) suggest that PWNe are responsible for the VHE emissions. The emissions from LHAASO J2226+6057 (57, 58) and eHWC J2019+368 (59), coincident with LHAASO J2018+3651, were also explored theoretically in the scenario of PWNe. However, none of the investigations are yet conclusive, and the competitive radiation mechanism has not been ruled out. Further measurements with better statistics are still highly desired.

4.3.2. Young massive star clusters. Young massive stars, which generate strong stellar winds, may densely cluster and form multiple shocks with the potential to accelerate CR protons to very high energies above 1 PeV (60). YMCs are recognized as major factories of Galactic CRs with much evidence in the VHE domain. The positional coincidence of LHAASO J2032+4102 with the YMC Cygnus OB2 provides further evidence that the YMC is a hadronic PeVatron. A recent report based on the HAWC observation also attributes the emissions at energies from 1 TeV to 100 TeV to the enclosed star-forming region Cygnus OB2 (61). Additional possible evidence may be from the positional coincidence of LHAASO J1849-0003 with W43. However, further in-depth morphological analysis is necessary to clarify the association based on future data collection.

4.3.3. Supernova remnants. SNRs, the spherical shock waves that expand in the interstellar medium (ISM) after the explosion of massive stars, have long been proposed as the most promising source of Galactic CRs.

The detection of γ-rays above 100 TeV from SNRs would give clues on the acceleration capability limit of SNRs at the highest energy, which is crucial to understanding the origin of CRs in the knee region. In the VHE domain, all the SEDs of young SNRs appear to be quite steep or have breaks at energies below 10 TeV. This has raised doubts about the ability of SNRs to operate as PeVatrons (60). More details about SNRs as PeVatron candidates can be found in a recent review article (62).

Among the LHAASO UHE sources, 6 out of 12 are found to have an SNR in their vicinity. However, most of the spatial coincidences are competing with energetic pulsars, and usually the PWN scenarios are preferred. The most favorable PeVatron candidate would be LHAASO J2226+6057, which is likely associated with SNR G106.3+2.7. A detailed discussion of the recent progress concerning the SNR G106.3+2.7 region can be found in Section 6.2. It is worth noting that further morphological analysis of this source in the UHE band in the near future might provide crucial information for PeVatron identification.

4.3.4. Microquasars. A microquasar consists of a binary system of a compact object (either a black hole or a neutron star) that accretes matter from a companion star. Such a miniature system can display some of the properties of quasars with relativistic jets. Observation of γ-rays from jets could provide valuable probes of the particle acceleration mechanisms in the jets. A

few of those objects (e.g., Cygnus X-1, Cygnus X-3) have been detected with γ-ray emissions in the high-energy band by AGILE and Fermi-LAT (see 63 and references therein). The γ-ray with the highest energy around 20 TeV was detected by HAWC from the jets of the microquasar SS 433 (64); therefore, microquasars could be PeVatron candidates. However, SS 433 is in the vicinity of the very extended source LHAASO J1908+0621, which is so bright that some contamination might be expected and needs to be carefully disentangled in the analysis of SS 433. The microquasar Cygnus X-3 has a similar problem because it is almost in the heart of a very complex extended source in the Cygnus region. Even worse, there is a very bright source, LHAASO J2032+4102, nearby as well. Not only are multiwavelength morphological analyses of those sources very necessary, but also the temporal structure of the emissions, particularly in the UHE regime, would play a crucial role in further detailed investigation. Such a combined analysis may shed light on the identification of microquasars as PeVatron candidates.

5. THE CRAB NEBULA: AN EXTREME ELECTRON ACCELERATOR AND A POTENTIAL SUPER-PEVATRON

In this section, we discuss the Crab Nebula as the first well-studied PeVatron. We analyze the potential for astrophysics discovery and the impact on γ-ray astronomy through targeted observations of this special lepton PeVatron.

On July 4, 1054, Chinese astronomers recorded the supernova that evolved into today's Crab Nebula, the best-observed high-energy astrophysical object. The ejecta forms the remnant with a size of approximately 11 light-years (ly). The central pulsar with a spin period of 33 ms powers a strong electron–positron pair wind with a spin-down luminosity of 4.6×10^{38} erg s^{-1}. This forms a clear torus structure of termination shock fronts at a radius of 0.59 ly (inner) and 1.49 ly (outer). They are very bright in the X-ray band; not only the rings but also the clear structure of knots and a pair of jets indicate regions of strong radiation. All of these, together with the diffuse radiative region surrounding the pulsar, form a nebula of approximately 3 ly (65).

A relevant feature of the Crab Nebula is that its radiation covers nearly the whole electromagnetic wavelength range from radio waves to the highest γ-rays at approximately 1 PeV. The one-zone leptonic model roughly describes the main feature of the SED over 22 orders of magnitude by assuming a bulk of electrons, confined by an average magnetic field of approximately 100 μG, emitting photons up to 1 GeV via the synchrotron radiation and generating higher-energy γ-rays through the IC scattering process, as shown in **Figure 4*a***. However, statistical testing of the agreement between the model and data shows systematic deviations in almost all specific bands—for instance, the whole energy range covered by Fermi-LAT and particularly the UHE band. The strong systematic deviation indicates the possible existence of new components.

5.1. Facts and Challenges

The first evidence of UHE photon emission from the Crab Nebula was from the HAWC (71), Tibet ASγ (47), and MAGIC (52) experiments via use of various techniques. A few UHE photons have been collected.

Systematic observation has been done by LHAASO (33), which collected 89 UHE photons from the Crab Nebula, including two photons at 0.9 and 1.1 PeV. Together with the photons measured by LHAASO-WCDA and LHAASO-KM2A at lower energies, a log-parabola spectrum over three decades of energy clearly reveals the radiation feature of the Crab Nebula in the UHE domain. The PeV photons are measured with negligible probabilities of CR background contamination.

Assuming the PeV photons are being generated by electrons, a few characteristics may be summarized as follows: (*a*) The parent electron must have an energy of 2.3 PeV, (*b*) the smallest

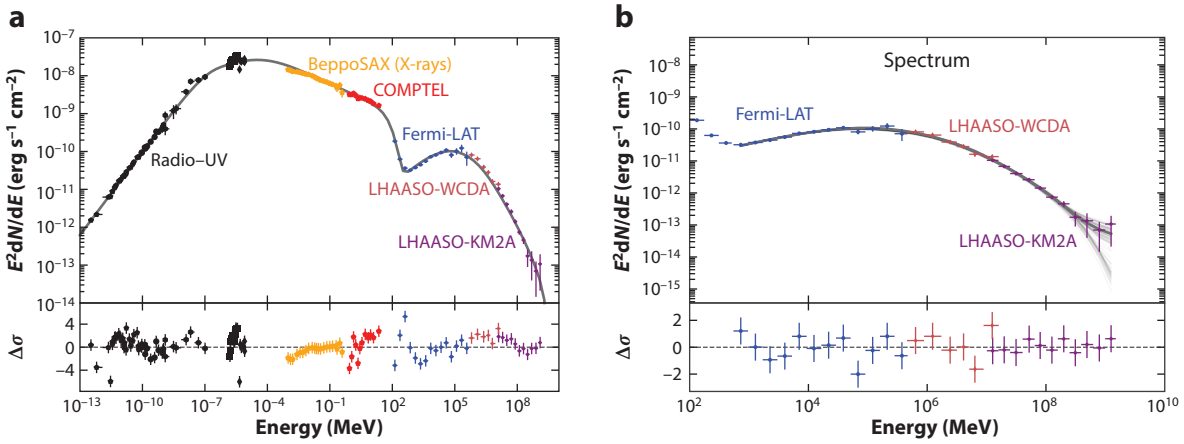

Figure 4

(*a*) SED of the Crab Nebula fitted with a simple one-zone electron model; different colors indicate the experiments that contributed the data in different bands (66–70). The lower subpanel shows the deviation of the model from the data. (*b*) The upper subpanel shows the combined SED of the Crab Nebula with data from Fermi-LAT, LHAASO-WCDA, and LHAASO-KM2A. The SED is well fitted above 1 GeV using a hybrid model with the "standard" one-zone lepton component plus a high-energy proton component, indicated by the shaded gray curves. The lower subpanel plots the deviation of the model from the data. A rather good agreement is clearly shown in this plot. Abbreviations: KM2A, 1-km^2 array; SED, spectral energy distribution; WCDA, water Cherenkov detector array. Figure adapted with permission from Reference 72.

region for those electrons to be confined in the magnetic field of 110 μG is 0.08 ly, and (*c*) the acceleration rate could be as high as 16%, which is a factor of 1,000 higher than the diffuse shock acceleration in SNRs.

The SED analysis demonstrates that the one-zone model may be too simple. Systematic deviations $>10\sigma$ are found in various bands from radio waves to UHE γ-rays. From 1 GeV to 1 PeV, the γ-ray spectrum could be much better fitted by introducing the second component of sources, either electrons or protons (e.g., 72). It was found that the systematic deviations are nearly completely removed in the SED fitting over the whole γ-ray band by simply introducing a proton component for the spectrum above 300 TeV, as shown in **Figure 4*a***.

Many advances have been made in modeling the Crab Nebula based on magnetohydrodynamic calculations using the particle-in-cell technique by various research groups (73–75). Many details of plasma evolution, the terrain of the shock front, and particle acceleration have been revealed in one- and two-dimensional simulations. The capacities of modern computing facilities have enabled exploration even in the three-dimensional domain. This has helped us understand how particles are accelerated by allowing us to trace them through the tabulating plasma. Some fundamental questions, such as the extremely large acceleration rate observed in the Crab Nebula, remain open. It is still challenging to understand the acceleration of electrons up to the level of 1 PeV (76). The lower-energy radiation, in the bands of radio and GeV γ-rays, would not be explained well in the same theoretic frame if the initial conditions of the simulations were overoptimized for generating the extremely high-energy photons.

5.2. A Super-PeVatron of Protons?

Although it is generally believed that most of the rotational energy of pulsars reduced during spin-down is converted into the energy of electron–positron pairs and magnetic fields in PWNe, protons also can be loaded in the pulsar wind and accelerated to high energies. In fact, some studies

over the past several decades have discussed proton acceleration and pionic γ-ray signatures in PWNe, especially in the Crab Nebula (e.g., 58, 72, 77–84). The possible SED structure of the Crab Nebula at the highest energy, which is yet to be statistically significantly confirmed in LHAASO's observation, may be accounted for by the hybrid model of a "standard" one-zone leptonic origin plus a very energetic proton component with a cutoff at energies $\gtrsim$10 PeV, as shown in **Figure 4*b***. Using the last two data points as upper limits to constrain the flux of the hadronic component, one finds that protons could take up to 10–50% of the released rotational energy if taking into account that protons injected at early time have escaped the nebula (85). If each pulsar in our Galaxy converted a comparable fraction of rotational energies to protons, pulsars might potentially explain the CR flux in the range of 10 to 100 PeV.

6. THE GALACTIC COSMIC RAY FACTORIES

SNRs are believed to be the most prominent CR accelerators in our Galaxy. AGILE (86) and Fermi-LAT (16) have revealed distinct low-energy breaks in the γ-ray spectrum in middle-aged SNRs (with an age of about 10,000 years). Such spectral features are regarded as decisive proof that SNRs accelerate CRs. On the other hand, GeV and TeV γ-ray observations also found that YMCs such as Cygnus OB2 (60, 61, 87), Westerlund 1 (88), and Westerlund 2 (89, 90) are also potential CR accelerators. Furthermore, the spectral feature reveals that these YMCs can even be promising PeVatron candidates (60). In this section, we summarize the current status and discuss the prospects of the UHE observations of those objects.

6.1. Cygnus Region: An Ideal Astrophysics Lab

YMCs have long been regarded as candidates for CR accelerators (91). Thanks to advances in γ-ray instruments, nearly a dozen YMCs have been detected in γ-rays (87–90, 92–94). Among them, the Cygnus region, because of its proximity and high luminosity, is the best-studied YMC system. The Cygnus region is one of the most intensive and nearby (at a distance $\approx$1.4 kpc) star-forming regions in our Galaxy. It harbors several Wolf–Rayet and hundreds of O-type stars grouped in powerful OB associations. It also contains huge HI and molecular gas complexes with total mass $>10^6 M_\odot$. TeV γ-rays have already been detected by HEGRA (95) and are the first unidentified source in the γ-ray band. Fermi-LAT detected high-energy (GeV) γ-rays from the direction of the most massive star association, Cygnus OB2. The source with an approximately 2° extension [called the Cygnus Cocoon (87)] has subsequently been detected in the TeV band as well (61, 96). The SED of the cocoon shows a hard spectrum (with an index of about 2.2) below 1 TeV and a gradual softening in the TeV band. Such a spectral feature can be explained by either propagation effects assuming a recent injection within 0.1 million years or a cutoff in the injected CR spectra (61). Furthermore, the CR spatial distribution derived from both the GeV and TeV γ-ray surface brightness (60, 61) and gas distributions in the Cygnus Cocoon obeys a $1/r$ profile, which is consistent with the continuous injection of CRs, where r is the distance to Cygnus OB2, the most probable CR accelerator in this region. Cygnus OB2 is one of the most powerful YMCs in our Galaxy; it consists of more than 50 O-type stars, and the total wind mechanical power is estimated to be 10^{39} erg s^{-1}. Assuming a reasonable acceleration rate (10%), when combining the size of the Cygnus Cocoon and the derived CR energy density profile, the diffusion coefficient inside the cocoon is estimated to be at least a factor of 100 smaller than the fiducial value in the GP (60).

Above 100 TeV, the HAWC observations did not show a significant cutoff; thus, we expect that such extended structure should also be detected in the UHE band. Recently, the Tibet ASγ Collaboration reported UHE γ-ray emissions from the Cygnus region (97), where only two compact sources are detected. However, it should be noted that in the diffuse emissions detected by Tibet

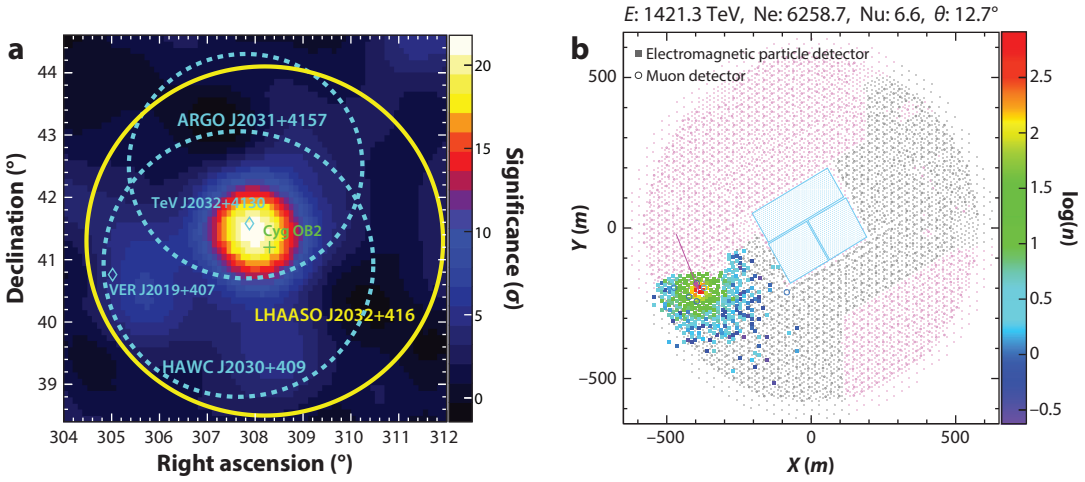

Figure 5

(*a*) Significance map of the Cygnus region above 25 TeV observed by LHAASO. The blue diamonds mark the TeV sources TeV J2032+4130 and VER J2019+407. The two blue dashed circles indicate two very extended sources, ARGO J2031+4157 and HAWC J2030+409. The yellow circle marks the source LHAASO J2032+416. (*b*) Charge distribution for the highest-energy γ-ray event (1.4 PeV) detected by LHAASO from the Cygnus region. Abbreviations: Ne, number of electromagnetic particles detected by electromagnetic particle detectors; Nu, number of muons detected by muon detectors. Figure adapted with permission from Reference 99.

ASγ, at least four UHE photons are in the vicinity of the Cygnus region (98). Remarkably, the highest-energy photon detected so far, a photon of 1.42 ± 0.13 PeV (which is a clear identification of a photon-initiated shower with 0.028% probability of being induced by a background CR), was found from LHAASO J2032+4102 (**Figure 5**), an extended UHE source in the direction of the Cygnus region (7). This makes it the most promising PeVatron candidate and provides a strong indication of a super-PeVatron that produces CRs above 10 PeV in our Galaxy.

An obvious question is whether the measured size of the Cygnus Cocoon is a physical boundary or is just caused by the limited sensitivity of instruments. Indeed, in the continuous injection scenario, the $1/r$ CR profile predicts a dimmer surface brightness at large r values. It is possible that more sensitive instruments would reveal even more extended structures than the cocoon. In this regard, with the unprecedented sensitivity above 100 TeV and large field of view, LHAASO will provide unambiguous information on the γ-ray spectral and spatial properties in the Cygnus region, shed light on the origin of CRs, and facilitate identification of Galactic PeVatrons.

It is worth noting that the Cygnus region is a complex region crowded by the SNR Cygni, the γ-ray binary Cygnus X-3, and PSR J2032+4127, besides the YMC Cygnus OB2. Many new observations in the VHE and UHE bands are still unclear. For instance, the Carpet-2 experiment team (100) recently reported that the detection of a 3.1σ excess of γ-ray flux at energies >300 TeV might be associated with a 150-TeV neutrino event detected by IceCube (101) and is likely consistent with a flare with a duration of a few months. Therefore, adequate photon statistics provided by LHAASO for spectrometric and morphological studies of this region are expected to address many open questions related to PeVatrons in this region.

6.2. SNR G106.3+2.7 as PeVatron Candidate

G106.3+2.7 is a radio source identified as an SNR (102). It presents a complex morphology that generally can be divided into a compact head in the northeast part of the source and an elongated

tail extending toward the southwest. An energetic pulsar, PSR J2229+6114, is located in the northern part of the head region, surrounded by a boomerang-shaped radio nebula. The latter is named after its morphology (i.e., the Boomerang Nebula) and is believed to be powered by PSR J2229+6114, which is of a characteristic age of 10 kiloyears and has a spin-down luminosity of 2.2×10^{37} erg s^{-1}. Although it has not been concretely confirmed, the Boomerang Nebula and SNR G106.3+2.7 are usually considered to have been born from the same supernova explosion. The distance of the system is suggested to be 0.8 kpc (103), based on the apparent spatial correspondence between the radio contour and the distribution of the HI emissions around the head region. It appears that the SNR head including the Boomerang Nebula is interacting with ambient atomic hydrogen gas while the SNR tail is expanding into a cavity. However, a much farther distance of 3 kpc from the source is proposed (104) based on the hydrogen column density obtained from the X-ray spectral fitting of PSR J2229+6114. This could imply a different scenario of the radiation mechanism.

This SNR-PWN complex has been detected in the γ-ray band from approximately 1 GeV to hundreds of TeV by various instruments (7, 105–110), as shown in **Figure 6**. Fermi-LAT detected an extended source with a radius of 0.25° in the tail region, which is in spatial coincidence with a molecular cloud (110, 111). Such an association is corroborated by the observation of Tibet ASγ in 6–115 TeV (105). LHAASO's measurement (7) in the UHE band shows a source centroid consistent with the position of the SNR tail, while the spatial extension of the source also covers the head region. The spectrum measured by LHAASO extends up to 500 TeV without an obvious cutoff feature. A simple one-zone leptonic model cannot explain the broadband γ-ray spectrum because the IC radiation of electrons at high energies is suppressed by the Klein–Nishina effect.

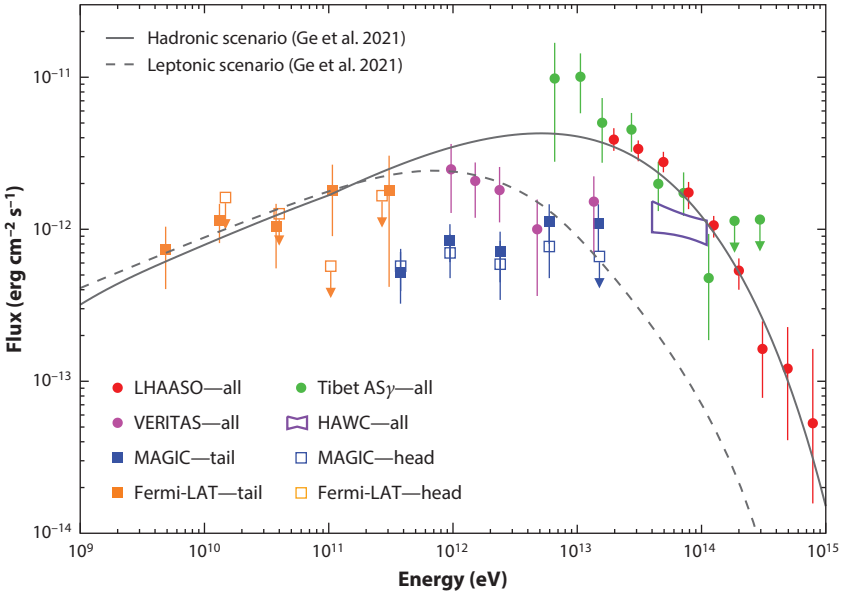

Figure 6

GeV–PeV γ-ray spectral energy distribution of the G106.3+2.7 region measured by various instruments. The solid and dashed curves show for reference the expected flux with the simple one-zone model in the hadronic scenario and the leptonic scenario, respectively, given by Reference 113. LHAASO data from Reference 7. Tibet ASγ data from Reference 105. HAWC data from Reference 106. VERITAS data from Reference 109. MAGIC data from Reference 116. Fermi-LAT data from References 110 and 117.

Both the spectral and the morphological measurements seem to favor a hadronic origin of the γ-ray emissions in the SNR tail, implying the existence of a proton PeVatron in this region.

The most plausible PeVatron candidate is the SNR shock, from which accelerated protons may escape and illuminate the molecular cloud (112). Nonthermal X-ray emissions have been discovered from the tail region (113, 114); these are emitted by electrons accelerated in situ according to the X-ray intensity profile (113). The X-ray indicates a high shock velocity of at least several thousands of kilometers per second presented in the tail region (115), making possible the acceleration of PeV protons from the SNR shock. If the Boomerang Nebula and SNR G106.3+2.7 are truly associated, the high shock velocity makes the SNR quite unusual given its age inferred from the pulsar. It is speculated that the shock in the tail direction has not been decelerated since it is expanding in a low-density cavity (113), which may be created by the stellar wind or supernova explosion of previous generations of stars (103). Acceleration of PeV protons might be related to such a special environment, which makes the SNR shock maintain a high speed for a long time.

7. PULSAR HALOS

Pulsar halos are believed to be formed by the pulsars alone with the associated SNRs disappearing either because of proper motions of the pulsars out of the SNRs or from the SNRs fading away (118). This generally begins at approximately 100 kiloyears after the birth of a pulsar. Pulsar halos have been discovered to be VHE γ-ray sources with spectra likely extending to the UHE regime. In this section, we briefly introduce the observations of HAWC and LHAASO as well as the underlying physics of pulsar halos. Readers may refer to recent reviews (119–121) for detailed discussions.

Discovery of extended multi-TeV γ-ray emission around the Geminga pulsar (PSR J0633+1746) and the Monogem pulsar (PSR J0659+1414) by HAWC (122) indicates that the PWNe of these two middle-aged pulsars remain efficient particle accelerators and inject a considerable amount of ultrarelativistic e^+e^- pairs into the ambient ISM. Similar to PWNe, the spatially extended γ-ray emissions of pulsar halos are also produced by IC radiation of electron–positron pairs having escaped to the ISM. This is different from PWNe, where e^+e^- pairs are confined in PWNe, which are much smaller regions than halos. The spectra of pulsar halos measured by HAWC continue up to 40 TeV without clear cutoff features. This indicates injection of pairs with energies >100 TeV from the pulsars. The sizes of sources are at least 20–30 pc, which is about two orders of magnitude larger than the typical size of a bow-shock PWN. Hence, they are regarded as a new category of γ-ray sources and are termed pulsar halos or TeV halos. Intriguingly, the steep declining profiles of the surface brightness with the distance from the pulsars measured by HAWC suggest a diffusion coefficient of particles inside the halos two to three orders of magnitude lower than the average diffusion coefficient in ISM derived from measurements of the ratio between secondary and primary CRs (123). The origin of such a slow diffusion is still unclear and under debate.

Since the Geminga pulsar and the Monogem pulsar are not unique, one may expect halos to exist around other middle-aged pulsars (124, 125). HAWC and LHAASO have detected some extended sources in spatial association with energetic pulsars of comparable ages to these two pulsars. However, many of these cannot be unambiguously identified as pulsar halos yet. Among them, the most promising is the extended source LHAASO J0621+3755 (126), where a middle-aged pulsar, J0622+3749, is located at the center of the source. The pulsar has the characteristic age, rotation period, and spin-down power (208 kiloyears, 0.333 s, and 2.7×10^{34} erg s^{-1}, respectively) comparable to those of the Geminga pulsar (342 kiloyears, 0.237 s, and 3.3×10^{34} erg s^{-1}) and the Monogem pulsar (110 kiloyears, 0.385 s, and 3.8×10^{34} erg s^{-1}). No other plausible astrophysical counterpart is found in the region around this source. Fitting the morphology with

a two-dimensional Gaussian template, a radius of 0.6° is found to contain 68% photon flux from the source, corresponding to a spatial size that could be 17 pc according to the distance of the pulsar about 1.6 kpc. It is worth noting that the distance is estimated based on the correlation between the γ-ray luminosity and the spin-down power of γ-ray pulsars (127). The physical size is comparable to that of the halos of Geminga and Monogem, although the angular size is much smaller. However, current data do not support a statistically significant claim for identification. One may have to wait a couple of years for a decisive conclusion on this source.

One key issue in understanding pulsar halos is the origin of the slow diffusion of injected e^+e^- pairs. An intuitive interpretation is the existence of a highly turbulent interstellar magnetic field around those middle-aged pulsars. The strong turbulence could be either extrinsically driven at small scales (128) or self-generated by particles themselves via the streaming instability (129, 130). Alternatively, a low-level turbulence scenario may explain the slow diffusion given the small inclination angle between the average magnetic field direction and the observer's line of sight (131). In this case, the required slow diffusion can be ascribed to the cross-field diffusion of CRs, which is largely suppressed. So far, a consensus has not been reached on the origin of the slow diffusion (132–134). It is suggested that the operation of LHAASO for several years would make it possible to distinguish different scenarios (133). On the other hand, the multiwavelength observations combining those in the GeV γ-ray band (135, 136) and the X-ray band (137) are also helpful in understanding the nature of pulsar halos.

8. DIFFUSE ULTRA-HIGH-ENERGY GAMMA-RAY EMISSION FROM THE GALACTIC PLANE

Galactic CRs are expected to be accelerated by sources in the GP. The average gas density in the GP also is believed to be much higher than in the Galactic halo. Thus, both the higher CR intensity and the gas density predict that the GP should be a bright γ-ray emitter. Indeed, the bright diffuse γ-ray emission in the GP is one of the most prominent features in the GeV γ-ray sky (138). At higher energies, the diffuse emission is also detected by the EAS arrays, Milagro (139) and ARGO-YBJ (140). The Milagro measurement extends the SEDs of diffuse γ-ray emissions to approximately 15 TeV, and the fluxes are consistent with the prediction made using the GALPROP code. HESS also detected diffuse γ-ray emissions around 1 TeV (141). However, because of its limited field of view and the background subtraction method, HESS can hardly resolve the large-scale variation in diffuse emissions such as Galactic IC emissions.

Galactic diffuse γ-ray emissions are regarded as an important tool to trace the propagation of Galactic CRs. For PeV CRs, the diffuse γ-ray emissions above 100 TeV are crucial. Recently, the Tibet ASγ experiment reported the first detection of diffuse γ-ray emissions above 100 TeV (98). Remarkably, 38 γ-like events above 398 TeV were detected in the GP without association with any known source. This may indicate the existence of CRs beyond a few PeV in the GP. The measured γ-ray flux above 398 TeV is slightly higher than the prediction by models such as GALPROP (98). However, whether those photons are associated with the isolated CR sources is not clear given the statistical constraints of the instrument's sensitivity. Conventionally, the diffuse emissions are believed to be produced by the interaction of a relatively uniform CR "sea" with gases. However, as mentioned in Reference 142, the CRs that escape from the sources produce very extended γ-ray emissions. In this regard, although the UHE photons detected by Tibet ASγ are far from known TeV sources, there still is some probability that they are from sources not resolvable by the Tibet ASγ detector.

The straightforward way to pin down such ambiguity is either to resolve those sources with more sensitive detectors, such as LHAASO, or to improve the measurements of diffuse emissions in the entire UHE domain. This requires not only much significant detection of diffuse emissions

but also the ability to distinguish between photons from the true diffuse emissions and those from discrete faint sources. Recently finished analyses of LHAASO observations on both the UHE diffuse γ-ray distribution in the Northern Sky (143) and the catalog of UHE sources (144) represent a first step toward the goal of precise measurements.

9. SUMMARY

By discovering more than a dozen UHE γ-ray sources, LHAASO has thoroughly opened the window of UHE γ-ray astronomy. Those sources reveal that our Galaxy is full of powerful particle accelerators known as PeVatrons, thus shedding light on the puzzle of the origin of CRs. The possible astrophysical counterparts of the PeVatrons are diverse and include PWNe, SNRs, and star-forming regions. These developments greatly enrich the UHE astronomy and strongly imply that CRs are sources from various types of factories.

Among the sources, the Crab Nebula is the only one that has been firmly localized and identified. In-depth investigation with the hundreds of UHE photons reveals that the Crab Nebula is an extreme electron PeVatron, accelerating particles at a rate close to the theoretical limit. Moreover, the SED in the UHE band, around 1 PeV in particular, indicates a deviation from the standard one-zone leptonic model and provides a hint of a hadronic component.

In conclusion, UHE γ-ray astronomy opens a wide field for further exploration of new radiation mechanisms and, more importantly, exploration of CR particle acceleration and propagation within source regions. Observation of diffuse γ-ray distribution will provide essential information about the transportation of the CRs in our Galaxy, which is related to the origin of the knee structure of the CR spectrum. Furthermore, UHE γ-ray observation opens up a new energy domain for indirect searches of dark matter (145) and tests of fundamental physics laws (146), which will help us explore potential new physics in unprecedented parameter spaces. This review was motivated by reviewing the status of the completely new field of UHE γ-ray astronomy, but it will likely raise a series of questions to be addressed in future investigations.

DISCLOSURE STATEMENT

The authors are not aware of any affiliations, memberships, funding, or financial holdings that might be perceived as affecting the objectivity of this review.

ACKNOWLEDGMENTS

This work was funded by the National Key R&D Program of China under grants 2018YFA0404204 and 2018YFA0404201, the Chengdu Management Committee of Tianfu New Area, and the Natural Science Foundation of China under grants 12022502 and U2031105. The authors also appreciate the proofreading and efforts to improve the English-language presentation of the manuscript by Andrew J. Cao.

LITERATURE CITED

1. Hinton JA, Hofmann W. *Annu. Rev. Astron. Astrophys.* 47:523 (2009)
2. Weekes TC, et al. *Astrophys. J.* 342:379 (1989)
3. Funk S. *Annu. Rev. Nucl. Part. Sci.* 65:245 (2015)
4. Samorski M, Stamm W. *Astrophys. J. Lett.* 268:L17 (1983)
5. Cao Z. *Universe* 7:339 (2021)
6. Cao Z. *Nat. Astron.* 5:849 (2021)
7. Cao Z, et al. *Nature* 594:33 (2021)

8. Moskalenko IV, Porter TA, Strong AW. *Astrophys. J. Lett.* 640:L155 (2006)
9. Popescu CC, et al. *Mon. Not. R. Astron. Soc.* 470:2539 (2017)
10. Franceschini A, Rodighiero G, Vaccari M. *Astron. Astrophys.* 487:837 (2008)
11. Gould RJ, Schréder G. *Phys. Rev. Lett.* 16:252 (1966)
12. Bartoli B, et al. *Phys. Rev. D* 92:092005 (2015)
13. Blasi P. *Astron. Astrophys. Rev.* 21:70 (2013)
14. Kelner SR, Aharonian FA, Bugayov VV. *Phys. Rev. D* 74:034018 (2006)
15. Giuliani A, et al. *Astron. Astrophys.* 516:L11 (2010)
16. Ackermann M, et al. *Science* 339:807 (2013)
17. Acero F, et al. *Astron. Astrophys.* 516:A62 (2010)
18. Aharonian F, et al. *Astron. Astrophys.* 464:235 (2007)
19. Archambault S, et al. *Astrophys. J.* 836:23 (2017)
20. Ahnen ML, et al. *Mon. Not. R. Astron. Soc.* 472:2956 (2017)
21. Abramowski A, et al. (HESS Collab.) *Astrophys. J. Lett.* 794:L1 (2014)
22. Abu-Zayyad T, et al. *Astrophys. J.* 557:686 (2001)
23. Berezinsky V, Gazizov A, Grigorieva S. *Phys. Rev. D* 74:043005 (2006)
24. Grenier IA, Black JH, Strong AW. *Annu. Rev. Astron. Astrophys.* 53:199 (2015)
25. Bartoli B, et al. *Phys. Rev. D* 84:022003 (2011)
26. Yodh GB. *Space Sci. Rev.* 75:199 (1996)
27. Abeysekara AU, et al. *Astropart. Phys.* 50:26 (2013)
28. LHAASO Collab. *Chin. Phys. C* 34:249 (2010)
29. Cao Z, et al., eds. arXiv:1905.02773 [astro-ph.HE] (2019)
30. Krimm HA, et al. *AIP Conf. Proc.* 220:122 (1991)
31. Amenomori M, et al. *AIP Conf. Proc.* 220:257 (1991)
32. Amenomori M, et al. *Astrophys. J.* 813:98 (2015)
33. Cao Z, et al. (LHAASO Collab.) *Science* 373:425 (2021)
34. Sako TK, et al. *Astropart. Phys.* 32:177 (2009)
35. Bartoli B, et al. *Astrophys. J.* 779:27 (2013)
36. DeYoung T. (HAWC Collab.) *Nucl. Instrum. Methods Phys. Res. A* 692:72 (2012)
37. Cao Z, et al. *Chin. Astron. Astrophys.* 43:457 (2019)
38. Bernlöhr K, et al. *Astropart. Phys.* 43:171 (2013)
39. de Angelis A, Mansutti O, Persic M. *Nuovo Cim. Riv. Ser.* 31:187 (2008)
40. Tescaro D. *Nucl. Instrum. Methods Phys. Res. A* 766:65 (2014)
41. Ajello M, et al. *Astrophys. J. Suppl.* 256:12 (2021)
42. Albert A, et al. (HAWC Collab.) *Astrophys. J.* 905:76 (2020)
43. Aharonian F, et al. *Chin. Phys. C* 45:025002 (2021)
44. Pintore F, et al. *J. High Energy Astrophys.* 26:83 (2020)
45. Hinton J. (SWGO Collab.) *Proc. Sci.* ICRC2021:023 (2022)
46. Abramowski A, et al. (HESS Collab.) *Nature* 531:476 (2016)
47. Amenomori M, et al. *Phys. Rev. Lett.* 123:051101 (2019)
48. Abeysekara AU, et al. (HAWC Collab.) *Phys. Rev. Lett.* 124:021102 (2020)
49. Adams CB, et al. *Astrophys. J.* 913:115 (2021)
50. Aharonian F, et al. *Nature* 439:695 (2006)
51. Acciari VA, et al. (MAGIC Collab.) *Astron. Astrophys.* 642:A190 (2020)
52. Acciari VA, et al. (MAGIC Collab.) *Astron. Astrophys.* 635:A158 (2020)
53. Gaensler BM, Slane PO. *Annu. Rev. Astron. Astrophys.* 44:17 (2006)
54. de Oña Wilhelmi E, López-Coto R, Amato E, Aharonian F. *Astrophys. J. Lett.* 930:L2 (2022)
55. Burgess DA, et al. *Astrophys. J.* 930:148 (2022)
56. Albert A, et al. *Astrophys. J.* 928:116 (2022)
57. De Sarkar A, et al. *Astron. Astrophys.* 668:A23 (2022)
58. Liang XH, et al. *Universe* 8:547 (2022)
59. Fang J, Wen L, Yu H, Chen S. *Mon. Not. R. Astron. Soc.* 498:4901 (2020)

60. Aharonian F, Yang R, de Oña Wilhelmi E. *Nat. Astron.* 3:561 (2019)
61. Abeysekara AU, et al. *Nat. Astron.* 5:465 (2021)
62. Cristofari P. *Universe* 7:324 (2021)
63. Bodaghee A, et al. *Astrophys. J.* 775:98 (2013)
64. Abeysekara AU, et al. *Nature* 562:82 (2018)
65. Ng CY, Romani RW. *Astrophys. J.* 601:479 (2004)
66. Baars JWM, Hartsuijker AP. *Astron. Astrophys.* 17:172 (1972)
67. Bandiera R, Neri R, Cesaroni R. *Astron. Astrophys.* 386:1044 (2002)
68. Veron-Cetty MP, Woltjer L. *Astron. Astrophys.* 270:370 (1993)
69. Kuiper L, et al. *Astron. Astrophys.* 378:918 (2001)
70. Arakawa M, Hayashida M, Khangulyan D, Uchiyama Y. *Astrophys. J.* 897:33 (2020)
71. Abeysekara AU, et al. *Astrophys. J.* 881:134 (2019)
72. Nie L, Liu Y, Jiang Z, Geng X. *Astrophys. J.* 924:42 (2022)
73. Pétri J, Lyubarsky Y. *Astron. Astrophys.* 473:683 (2007)
74. Amato E, Olmi B. *Universe* 7:448 (2021)
75. Du S, et al. In *AGU Fall Meeting Abstracts*, Abstr. SM34B-05. Washington, DC: Am. Geophys. Union (2021)
76. French O, Guo F, Zhang Q, Uzdensky DA. *Astrophys. J.* 948:19 (2023)
77. Cheng KS, et al. *J. Phys. G* 16:1115 (1990)
78. Atoyan AM, Aharonian FA. *Mon. Not. R. Astron. Soc.* 278:525 (1996)
79. Amato E, Guetta D, Blasi P. *Astron. Astrophys.* 402:827 (2003)
80. Horns D, et al. *Astron. Astrophys.* 451:L51 (2006)
81. Zhang L, Yang XC. *Astrophys. J. Lett.* 699:L153 (2009)
82. Di Palma I, Guetta D, Amato E. *Astrophys. J.* 836:159 (2017)
83. Zhang X, Chen Y, Huang J, Chen D. *Mon. Not. R. Astron. Soc.* 497:3477 (2020)
84. Peng QY, Bao BW, Lu FW, Zhang L. *Astrophys. J.* 926:7 (2022)
85. Liu RY, Wang XY. *Astrophys. J.* 922:221 (2021)
86. Giuliani A, Cardillo M, Tavani M, et al. *Astrophys. J. Lett.* 742:L30 (2011)
87. Ackermann M, et al. *Science* 334:1103 (2011)
88. Abramowski A, et al. *Astron. Astrophys.* 537:A114 (2012)
89. Yang R-z, de Oña Wilhelmi E, Aharonian F. *Astron. Astrophys.* 611:A77 (2018)
90. Abramowski A, et al. (HESS Collab.) *Astron. Astrophys.* 525:A46 (2011)
91. Cesarsky CJ, Montmerle T. *Space Sci. Rev.* 36:173 (1983)
92. Yang R, Aharonian F, Evoli C. *Phys. Rev. D* 93:123007 (2016)
93. Sun XN, et al. *Astron. Astrophys.* 639:A80 (2020)
94. Yang RZ, Wang Y. *Astron. Astrophys.* 640:A60 (2020)
95. Aharonian F, et al. *Astron. Astrophys.* 393:L37 (2002)
96. Bartoli B, et al. (ARGO-YBJ Collab.) *Astrophys. J.* 790:152 (2014)
97. Amenomori M, et al. *Phys. Rev. Lett.* 127:031102 (2021)
98. Amenomori M, et al. *Phys. Rev. Lett.* 126:141101 (2021)
99. Li C. (LHAASO Collab.) *Proc. Sci.* ICRC2021:843 (2022)
100. Dzhappuev DD, et al. *Astrophys. J. Lett.* 916:L22 (2021)
101. IceCube Collab. GCN Circular 28927, NASA, Washington, DC (2020)
102. Pineault S, Joncas G. *Astron. J.* 120:3218 (2000)
103. Kothes R, Uyaniker B, Pineault S. *Astrophys. J.* 560:236 (2001)
104. Halpern JP, Gotthelf EV, Leighly KM, Helfand DJ. *Astrophys. J.* 547:323 (2001)
105. Amenomori M, et al. (Tibet ASγ Collab.) *Nat. Astron.* 5:460 (2021)
106. Albert A, et al. *Astrophys. J. Lett.* 896:L29 (2020)
107. Acciari VA, et al. (MAGIC Collab.) *Proc. Sci.* ICRC2021:796 (2022)
108. Abdo AA, et al. *Astrophys. J. Lett.* 664:L91 (2007)
109. Acciari VA, et al. *Astrophys. J. Lett.* 703:L6 (2009)
110. Xin Y, et al. *Astrophys. J.* 885:162 (2019)

111. Fang K, et al. *Phys. Rev. Lett.* 129:071101 (2022)
112. Bao Y, Chen Y. *Astrophys. J.* 919:32 (2021)
113. Ge C, et al. *Innovation* 2:100118 (2021)
114. Fujita Y, Bamba A, Nobukawa KK, Matsumoto H. *Astrophys. J.* 912:133 (2021)
115. Zirakashvili VN, Aharonian F. *Astron. Astrophys.* 465:695 (2007)
116. Abe H, et al. (MAGIC Collab.) *Astron. Astrophys.* 671:A12 (2023)
117. Liu RY, Yan H. *Mon. Not. R. Astron. Soc.* 494:2618 (2020)
118. Giacinti G, et al. *Astron. Astrophys.* 636:A113 (2020)
119. Liu RY. *Int. J. Mod. Phys. A* 37:2230011 (2022)
120. López-Coto R, et al. *Nat. Astron.* 6:199 (2022)
121. Fang K. *Front. Astron. Space Sci.* 9:1022100 (2022)
122. Abeysekara AU, et al. *Science* 358:911 (2017)
123. Amato E, Blasi P. *Adv. Space Res.* 62:2731 (2018)
124. Linden T, et al. *Phys. Rev. D* 96:103016 (2017)
125. Sudoh T, Linden T, Beacom JF. *Phys. Rev. D* 100:043016 (2019)
126. Aharonian F, et al. *Phys. Rev. Lett.* 126:241103 (2021)
127. Saz Parkinson PM, et al. *Astrophys. J.* 725:571 (2010)
128. López-Coto R, Giacinti G. *Mon. Not. R. Astron. Soc.* 479:4526 (2018)
129. Evoli C, Linden T, Morlino G. *Phys. Rev. D* 98:063017 (2018)
130. Mukhopadhyay P, Linden T. *Phys. Rev. D* 105:123008 (2022)
131. Liu RY, Yan H, Zhang H. *Phys. Rev. Lett.* 123:221103 (2019)
132. Fang K, Bi X-J, Yin P-F. *Mon. Not. R. Astron. Soc.* 488:4074 (2019)
133. Yan K, Liu RY, Chen SZ, Wang XY. *Astrophys. J.* 935:65 (2022)
134. De La Torre Luque P, Fornieri O, Linden T. *Phys. Rev. D* 106:123033 (2022)
135. Xi SQ, et al. *Astrophys. J.* 878:104 (2019)
136. Di Mauro M, Manconi S, Donato F. *Phys. Rev. D* 100:123015 (2019)
137. Liu RY, Ge C, Sun XN, Wang XY. *Astrophys. J.* 875:149 (2019)
138. Ackermann M, et al. *Astrophys. J.* 750:3 (2012)
139. Abdo AA, et al. *Astrophys. J.* 688:1078 (2008)
140. Bartoli B, et al. *Astrophys. J.* 806:20 (2015)
141. Abramowski A, et al. *Phys. Rev. D* 90:122007 (2014)
142. Yang R. *Sci. Sin. Phys. Mech. Astron.* 52:229501 (2022)
143. Cao Z, et al. (LHAASO Collab.) arXiv:2305.05372 [astro-ph.HE] (2023)
144. Cao Z, et al. (LHAASO Collab.) arXiv:2305.17030 [astro-ph.HE] (2023)
145. Cao Z, et al. (LHAASO Collab.) *Phys. Rev. Lett.* 129:261103 (2022)
146. Cao Z, et al. *Phys. Rev. Lett.* 128:051102 (2022)

Annual Review of Nuclear and Particle Science

Volume 73, 2023

Contents

Errata

An online log of corrections to *Annual Review of Nuclear and Particle Science* articles may be found at http://www.annualreviews.org/errata/nucl